

# **ELECTRON SCATTERING FROM GASEOUS OCS( $^1\Sigma$ ): COMPARING COMPUTED ANGULAR DISTRIBUTIONS AND ELASTIC CROSS SECTIONS WITH EXPERIMENTS.**

F.A. Gianturco\*

*Department of Chemistry, The University of Rome La  
Sapienza and CNISM, Piazzale A. Moro 5, 00185 Rome, Italy.*

T. Stoecklin

*Laboratoire de Physico-Chimie Moleculaire, 351,  
Cours de la Libération, F-33405 Talence, France.*

Differential cross sections are computed for the title polar molecule using static interaction, exchange forces and correlation-polarisation effects as described in detail in the main text. The dipole effect is also reported via the dipole Born correction procedure and the final angular distributions are compared with existing experimental data. The shape and location of the prominent low-energy resonance are computed and compared with experiments. The comparison shows that the present treatment of the interaction forces and of the quantum dynamics can indeed afford good agreement between measured and computed quantities for a multielectron target as OCS.

---

\* Corresponding author; e.mail address: fa.gianturco@caspur.it. Fax: +39-06-4991.3306.

## I. INTRODUCTION

The carbon oxysulfide (OCS) molecule is well known to be of considerable importance for the role it plays in the carbon chemistry and sulphur chemistry chains of reactions in molecular astrophysics environments like those in the diffuse and dark interstellar clouds (DISC)[1]. It is also of interest in the realm of cold molecular plasmas because of its function as a reaction quencher into the plasma formation. It follows, therefore, that collisional processes induced by low-energy electrons in this molecular gas have triggered the interest of both experimentalists and theoreticians, intrigued by the possible role that the permanent dipole of this target molecule can play in characterizing the scattering attributes.

On the theoretical side, earlier calculations were carried out by Lynch et al.[2] using their continuum scattering model, with which they found the presence of a  $\Pi$  symmetry shape resonance around 1.15 eV and a sharp increase at threshold of the  $\Sigma$  symmetry partial cross section. The differential cross sections (DCSs) for elastic scattering and for vibrational excitations were measured by Sohn and coworkers [3], where the authors also observed a  $\pi^*$  resonance and a strong excitation of the bending mode associated to dipole coupling and to a possible bound state of  $(OCS^-)^*$ . Further measurements are due to Szmytkowski et al. [4] who measured the total, integral cross sections of the title molecule and confirmed a  $\Pi$ -type resonance around 1.15 eV. More recent measurements have been carried out by the Japanese group [5], who compared similar measurements with electrons and positrons as projectiles and confirmed the presence of the  $\pi^*$  resonance around 1.15 eV. The vibrational excitation of OCS has been measured by another study from the same group [6]. Calculations of elastic cross sections, integral and differential, and of the momentum transfer cross sections have been performed by Bettega et al. [7], who employed the Schwinger multichannel method with pseudopotentials within the static-exchange approximation and examined a range of energies from 5 to 50 eV.

A combined theoretical-experimental study has been conducted by Michelin et al. [8] who carried out both measurements and calculations in the energy regime from 0.4 eV to 600 eV. Further calculations of both integral and differential cross sections were reported very recently by Bettega et al. [9], who employed again the Schwinger multichannel method with pseudopotentials, adding the polarization interaction to their static-exchange initial scheme. A further "addendum" to the above results was recently published with regard to the  $\Sigma$ -symmetry partial cross sections [10].

In the present study we intend to discuss in some detail the behavior of the computed angular

distributions with respect to the available experiments over a very broad range of collision energies, using an entirely different method as that employed by the earlier, just as extensive, calculations of references [8, 9, 10]. The following Section describes briefly our theoretical and computational approach while Section III reports our results for both the partial integral cross sections and the differential cross sections. The last Section IV summarizes our present conclusions.

## II. THE THEORETICAL MODELLING

### A. The separable exchange representation

One of the major requests from accurate calculations of low energy electron-molecule scattering observables is the correct description of the non-local part of the interaction potential. For electronically elastic collisions, a physically realistic treatment usually starts with the static interaction and views the exchange potential as a correction to the latter due to the imposition of anti-symmetry on the total electronic wavefunction that describes the scattered electron plus the target bound electrons. Even in this case, however, the correct treatment of non-local forces for polyatomic molecules still represents a rather formidable task and therefore increasing use is being made of separate representations which expand the exchange kernel in terms of products of one-electron functions [11]. This approach will be adopted in the present paper, following our extension of this method to polyatomic molecular targets [12, 13]. It has the advantage of being a non-empirical method for treating exchange forces while still offering computational savings with respect to the exact solution of the integro-differential equations of non-local electron-molecular scattering theory [14]. The earlier work on separate exchange in electron collision with small diatomics has been rather encouraging since fairly small exchange basis sets added little more computer time than a local potential calculation [11, 12] and therefore we use such an approach on the linear polyatomic target of the present study.

One starts by approximating the exchange potential  $W(\mathbf{r}, \mathbf{r}_e)$  by the truncated separate form

$$W(\mathbf{r}, \mathbf{r}_e) \approx \sum_{\alpha, \beta}^N \chi_{\alpha}(\mathbf{r}) \mathbf{W}_{\alpha, \beta} \chi_{\beta}(\mathbf{r}_e) \quad (1)$$

where the  $\{\chi_{\alpha}\}$  now constitute an additional, new set of Cartesian GTOs not orthogonal to each other, nor to the occupied molecular orbitals (MOs) of the target SCF basis set which describes the ground state of the target molecule. The vector coordinates  $(\mathbf{r})$  and  $(\mathbf{r}_e)$  describe the positions of

the bound and of the scattered electrons, respectively. The  $W_{\alpha,\beta}$  now represents the two-electron interaction operator over the truncated, discrete basis.

When performing the separable expansion (1) care should be taken of how to specify the exchange basis functions  $\{\chi_\alpha\}$  in order to avoid taking too large an expansion so that the calculations become too massive or begin to suffer from linear dependency effects. We have carefully checked this aspect of the problem by analysing in each case the corresponding eigenvectors of the overlap matrix and modifying the basis set accordingly.

The required exchange matrix elements for the bound MOs of the target, taken to be a closed-shell structure, are therefore given by first calculating the following matrix elements, via a standard bielectronic subroutine

$$\tilde{\mathbf{B}}_{\gamma\tau} = \int d\mathbf{r} \int d\mathbf{r}_e \varphi_\gamma(\mathbf{r}) W(\mathbf{r}, \mathbf{r}_e) \varphi_\tau(\mathbf{r}_e) \quad (2)$$

In the above equation  $\{\varphi_\gamma\}$  denotes the set of doubly occupied self-consistent-field (SCF) target MOs. Hence, using (1) one can further write

$$\tilde{\mathbf{B}}_{\gamma\tau} = \sum_{\alpha,\beta}^N \int d\mathbf{r} \varphi_\gamma(\mathbf{r}) \chi_\alpha(\mathbf{r}) W_{\alpha,\beta} \int d\mathbf{r}_e \varphi_\tau(\mathbf{r}_e) \chi_\beta(\mathbf{r}_e) \quad (3)$$

our further compact the overlap integrals

$$\tilde{\mathbf{B}}_{\gamma\tau} = \sum_{\alpha,\beta}^N S_{\gamma\alpha} W_{\alpha,\beta} S_{\beta\tau} \quad (4)$$

One can finally obtain the bound-continuum scattering matrix from the separable representation by writing it down via the following product of the matrices already defined in the above equations:

$$\mathbf{W} = \mathbf{S}^{-1} \tilde{\mathbf{K}} \mathbf{S}^{-1} \quad (5)$$

where the  $S_{\gamma\alpha}$  are the overlap matrix elements between the additional GTO set and the original expansions describing the bound MOs.

## B. The scattering equations

Within a single-centre expansion (SCE) of the continuum wavefunction and of the interaction potential, the use of the present static-separable-exchange approximation gives rise to a set of coupled integro-differential equations

$$\left\{ \frac{d^2}{dr_e^2} + \frac{l(l+1)}{r_e^2} \right\} u_{ll_0}(r_e) = \sum_{l'} \left\{ U_{ll'}(r_e) u_{ll_0}(r_e) + \sum_{\alpha\beta} \Phi_\alpha^l(r_e) W_{\alpha\beta} \int dr \Phi_\beta^l(r) u_{ll_0}(r) \right\} \quad (6)$$

where

$$U_{ll'}(\mathbf{r}_e) = \int S_l^m(\hat{r}_e) V(\mathbf{r}_e) S_{l'}^{m'}(\hat{r}_e) d\hat{r}_e \quad (7)$$

and

$$\Phi_\alpha^l(r_e) = (r_e) \int d\hat{r}_3 \varphi_\alpha(\mathbf{r}_e) S_l^m(\hat{r}_e) \quad (8)$$

which integrates over real spherical harmonics to yield the radial part of each new GTO function.

Here the  $\varphi$ 's are the orbital used in equation (2).

Furthermore

$$S_l^{m,p}(\hat{r}_e) = \frac{i}{\sqrt{2}} \{ Y_l^m(\hat{r}_e) \pm (-1)^p Y_l^{-m}(\hat{r}_e) \} \quad (9)$$

with the parity index  $p=0$  or  $1$  and where the same equation (8) also holds for the  $r$  variable in (6).

One can now express the solution as a linear combination of homogeneous and inhomogeneous terms:

$$u_{ll_0}(r_e) = u_{ll_0}^0(r_e) + \sum_{\alpha} u_l^\alpha(r_e) C_{l_0}^\alpha \quad (10)$$

where

$$(k^2 - H_0^l) u_{ll_0}^0(r_e) = \sum_{l'} U_{ll'}(r_e) u_{ll_0}(r_e) \quad (11)$$

$$(k^2 - H_0^l) u_l^\alpha(r_e) = \sum_{l'} U_{ll'}(r_e) u_{l'}^\alpha(r_e) + \Phi_\alpha^l(r_e) \quad (12)$$

The coefficients  $C_{l_0}^\alpha$  are found to satisfy a set of linear equations

$$\sum_{\beta} A_{\alpha\beta} C_{l_0}^\beta = B_{\alpha l_0} \quad (13)$$

where

$$A_{\alpha\beta} = \delta_{\alpha\beta} - \sum_{\nu\gamma} W_{\alpha\gamma} \int \Phi_{\beta}^{\nu}(r_e) u_{\nu}^{\beta}(r_e) dr_e \quad (14)$$

and

$$B_{\alpha l_0} = \sum_{\nu\beta} W_{\alpha\beta} \int_0^{\infty} \Phi_{\beta}^{\nu}(r_e) u_{\nu l_0}^0(r_e) dr_e \quad (15)$$

The final numerical integration of the ensuing Volterra equations was then carried out as already described in Jain and Norcross [15].

### III. COMPUTED AND MEASURED CROSS SECTIONS

#### A. Computational details

The interatomic distances were fixed at their experimental values of  $R_{oc} = 2.196 a_0$  and  $R_{cs} = 2.941 a_0$ . The two components of the dipole polarisability tensor were taken also, in the asymptotic interaction, to be the experimental values:  $\alpha_0(R_{eq}) = 35.1 a_0^3$  and  $\alpha_2(R_{eq}) = 17.5 a_0^3$ . The above choice was dictated by our desire to realistically treat low-energy effects which are known to be strongly affected by polarisabilities.

To describe the target electrons in the neutral ground state we employed a double-zeta D95V basis set plus polarization orbitals as in the expansion described as D95V\* [16]. The obtained total energy was therefore -1020.4122528 hartrees, with a dipole of 0.32 a.u. and a quadrupole of 0.87 a.u., to be computed with the experimental values of 0.27 a.u. for the dipole [4]. No experimental value of the molecular quadrupole was found to be available.

The radial grid chosen for the Volterra integrals went from 0.005  $a_0$  to 10.0  $a_0$ , beyond which the integration was extended out to 1,000  $a_0$  using the asymptotic static multipoles plus the polarization potential. The multipolar went up to  $\lambda_{max}=70$  while the bound orbitals were expanded around the center of mass up to  $l_{max}=118$ .

Table I reports the additional GTO's employed to describe the separable exchange and used in the dynamical calculations outlined in the previous Section.

The single-center partialwave expansion of the discretized, continuum orbitals employed to treat exchange involved  $l_{max}=15$  for the  $\Sigma$  symmetry,  $l_{max}=20$  for the  $\Pi$  symmetry and  $l_{max}=15$  for the  $\Delta$  symmetry.

TABLE I: Basis set functions (types, locations and exponents) for the continuum orbitals.

location: on the O	on the C	on the S	on the Center of mass
$\Sigma$ :	$\Sigma$ :	$\Sigma$ :	$\Sigma$ :
<b>s</b> :8.0,4.0,2.0, 1.0,0.5,0.25	<b>s</b> :8.0,4.0,2.0, 1.0,0.5,0.25,0.12	<b>s</b> :8.0,4.0,2.0, 1.0,0.5,0.25,0.12	
<b>p<sub>z</sub></b> :2.0,1.0,0.5,0.25	<b>p<sub>z</sub></b> :2.0,1.0,0.5,0.25	<b>p<sub>z</sub></b> :2.0,1.0,0.5,0.25	
<b>d<sub>xz</sub></b> :1.0,0.5,0.25	<b>d<sub>xz</sub></b> :1.0,0.5,0.25,0.12	<b>d<sub>xz</sub></b> :1.0,0.5,0.25,0.12	
$\Pi$ :	$\Pi$ :	$\Pi$ :	$\Pi$ :
<b>p<sub>x</sub></b> :32.0,16.0,8.0, 4.0,2.0,1.0,0.5		<b>p<sub>x</sub></b> :32.0,16.0,8.0, 4.0,2.0,1.0,0.5	<b>p<sub>x</sub></b> :32.0,16.0,8.0,4.0, 2.0,1.0,0.5
<b>d<sub>xz</sub></b> :4.0,2.0,1.0,0.5,0.25		<b>p<sub>xz</sub></b> :4.0,2.0,1.0,0.5,0.25	<b>d<sub>xz</sub></b> :4.0,2.0,1.0,0.5,0.25
$\Delta$ :	$\Delta$ :	$\Delta$ :	$\Delta$ :
<b>d<sub>xx</sub></b> :16.0,8.0,4.0,2.0, 1.0,0.5,0.25		<b>d<sub>xx</sub></b> :16.0,8.0,4.0,2.0, 1.0,0.5,0.25	<b>d<sub>xx</sub></b> :16.0,8.0,4.0, 4.0,2.0,1.0,0.5
<b>f<sub>x<sup>2</sup>z</sub></b> :4.0,2.0,1.0,0.5,0.25		<b>f<sub>x<sup>2</sup>z</sub></b> :4.0,2.0,1.0,0.5,0.25	<b>d<sub>xz</sub></b> : 4.0,2.0,1.0,0.5,0.25

The above set of functions was the result of a series of numerical tests at a set of chosen energies where we increased the number and quality of the additional GTO's until the corresponding, final K-matrix elements varied by less than 0.1%.

### B. The integral cross section

The results reported by figure 1 analyze the partial and total integral, elastic cross sections (rotationally summed) for their overall energy dependence over the broad range of energies which is experimentally available [3, 4, 5], but we only report a comparison with some of the data in order not to crowd the figure excessively. We also show in the lower panel the energy behavior of the individual partial cross sections for the contributing partial symmetries.

It is reassuring to see that the present calculations follow closely the experimental findings from below 1.0 eV of energy and up to 100 eV: this is a rather good result considering the complexity of the molecule and the broad range of energies spanned by the calculations. Furthermore, we see that the resonance position is obtained reasonably well from our calculations, albeit with a

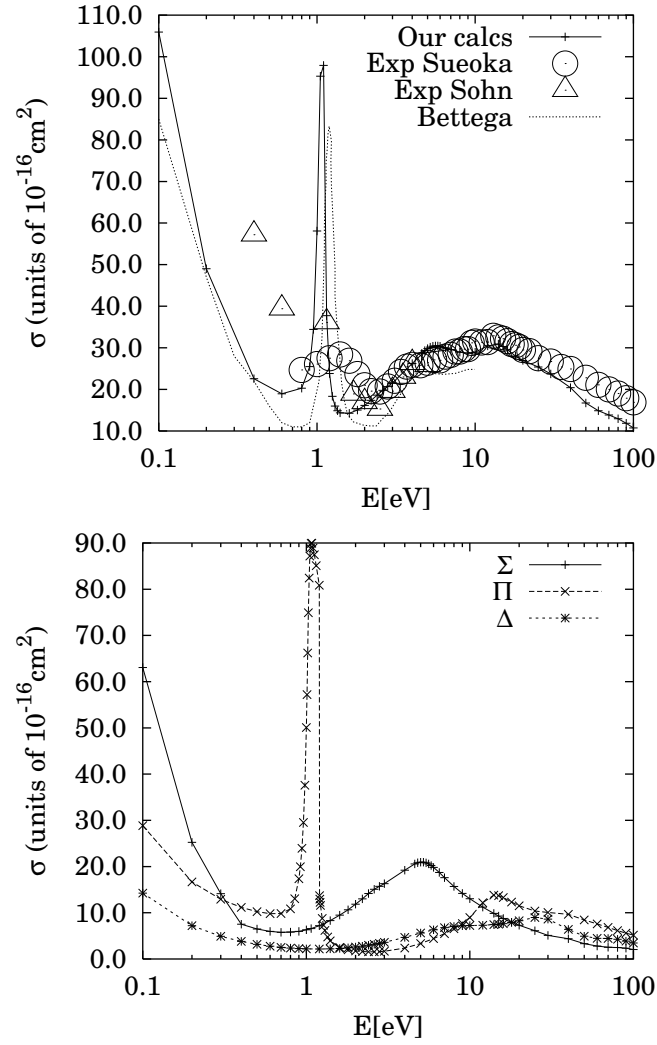


FIG. 1: Upper panel: Computed and measured total elastic integral cross sections as a function of energy. Solid line: present results; Dots: calculations from ref.[9]. Open circles: expt.s from ref.[3]; open triangles: expt.s from ref.[5]. Lower panel: partial cross sections for the  $\Sigma$ -(solid line),  $\Pi$ -(dashes) and  $\Delta$ -(dots) symmetries.

sharper peak due to the absence of vibrational averaging, which also come very close to the recent calculations of Bettega et al. [9] that employed an entirely different method for obtaining it.

The lower panel in the figure reports the energy dependence of the various partial cross sections which contribute to the scattering process. The calculations clearly show that:

1. the resonance around 1 eV is due to the  $\Pi$  symmetry i.e. to the expected dynamical (centrifugal) trapping of the electron into a  $\pi^*$  metastable orbital by the  $l=1$  angular momentum barrier;
2. there is a second  $\pi^*$  resonance at higher energies ( $\sim 10$  eV) which is a broader one and which



is also seen in the experimental data;

3. the  $\Sigma$ -symmetry exhibits the expected dominance of s-wave scattering as one moves down to low energies [10] and the corresponding cross section goes through a Ramsauer-Townsend minimum around 0.7 eV, as also analyzed and discussed by recent calculations of Bettega et al. [10];
4. the  $\Sigma$ -symmetry cross section also suggests the presence of a  $\sigma^*$  resonance around 4-5 eV which is also seen in the experiments (upper panel) as a shoulder on the rising cross section energy dependence around 4 eV. In Fig. 2 we report the behaviour of the eigenphase sum associated with the  $\Sigma$  symmetry component. We see that, at low energies, this quantity goes through zero, as in ref.[10], and therefore it suggests the presence of an RT minimum in the elastic cross section. It further increases from zero energy values and goes through a maximum as shown by similar data in ref.[10].

In conclusions, the present calculations for partial and total integral cross sections indicate that our present approach can reliably describe the experimental behavior over a very broad range of energies and can also reproduce earlier calculations very closely to their findings as far as partial symmetry contributions are concerned.

The previous literature [8, 9, 10] also discusses the possibility of having a virtual state close to zero energies detected by a negative value of the scattering length. Since the present system is a polar target, no modified effective range theory can be applied [16] and no scattering length could therefore be uniquely defined. Different procedures therefore need to be used to extract information on the possible existence of virtual states [18] in polar targets. In the present case, however, we decided that such a study was outside the scope of our current aims.

### C. Angular distributions at low energies

We have shown above that the well marked, low energy resonance appears, but in experiments and calculations, around 1 eV of collision energy, and therefore it becomes of interest to also see what the angular distributions look like across that range of energies. The results of our calculations, and their comparisons with the existing experiments, are shown in the

various panels of figure 3 and figure 4 where the energies vary from 0.4 eV up to 3.0 eV. The experiments are those of Sohn et al. [3] and from Tanaka [5], respectively marked by open circles and open triangles in all the panels, while the calculations (dashed curves) are from reference [8]. The following comments could be made:

- (a) at the lowest collision energies the scattering is dominated by the weak dipole interaction which causes a marked forward scattering behavior, which is also well reproduced by our calculations. On the other hand, in the larger angle region the agreement becomes less satisfactory, possibly due to our model treatment of short-range correlation effects. We also see that at 1.15 eV the earlier calculations [8] also do not agree well with experiments.
- (b) as the collision energy moves across the position of the strong  $\pi^*$  resonance, as shown by the panels of figures 3 and 4, we see that the angular distributions become much flatter from  $\vartheta \sim 20^\circ$  and out to  $140^\circ$ , with a markedly reduced forward peak, with the latter resuming as soon as the energy leaves the resonance region (e.g. see panels in figures 3 and 4).
- (c) We also see from Fig. 4 that, while the agreement with experiments is good at 2.0 eV, and remains reasonable at 2.5 - 3 eV, indicating numerical convergence of our present results to the same level of reliability with respect to the experiments.

In other words, we see the dominant presence of a forward scattering behavior of the DCSs unless we are at the resonance position, where the 'orbiting' features of the trapped electron distorts the effects coming from the permanent dipole of the target molecule.

#### **D. The DCSs at higher energies**

Since the experimental data for the angular distributions are available over a broad range of collision energies, we have analyzed them rather carefully from above the dominant  $\pi^*$  resonance out to about 100 eV. The comparisons with the measured data are shown in figures from 5 through 7. The following comments could be made from a perusal of the data shown in those figures:

1. the present calculations are seen to follow measurements remarkably well, both in shape and size, over the whole energy range;

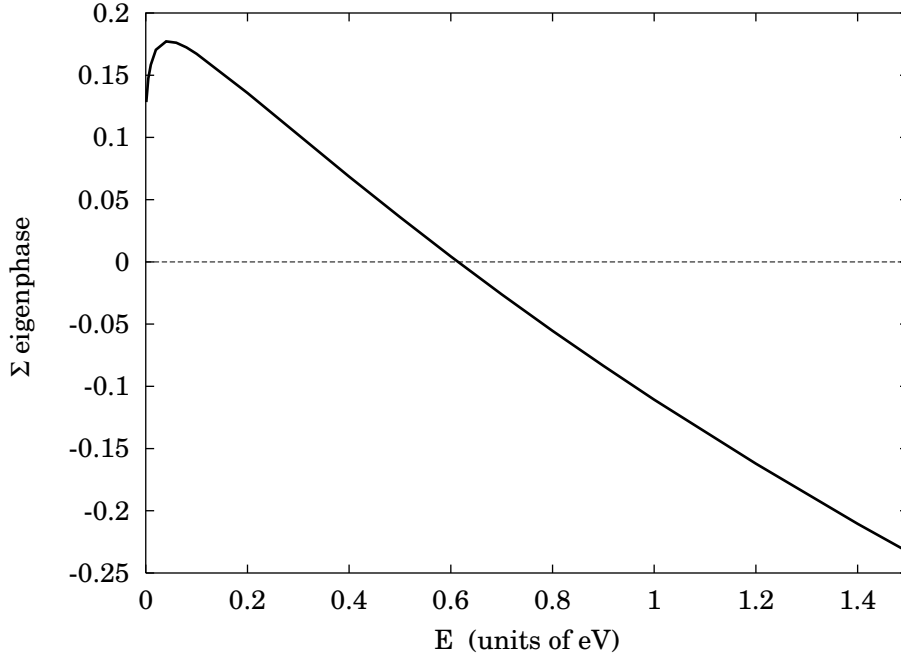


FIG. 2: Computed eigenphase sum behavior within the  $\Sigma$  symmetry component of the scattered electron.

2. at 5.0 eV the data from Sohn et al.[2] differ from those of Tanaka et al. [5] in the small-angle region since they indicate there a strong forward peaking of the angular distributions: our calculated values follow those measurements very accurately, thereby confirming the experimental findings in that angular regime;
3. as the collision energy increases one sees an increasing flattening of the DCSs as a function of the scattering angle and the appearance of the forward peaks at increasingly smaller angles: the calculations follow suit in the sense that indeed show the same general behavior as that indicated by the experiments.

#### IV. PRESENT CONCLUSIONS

The calculations discussed in this work have analyzed, using a quantum treatment of the scattering dynamics, the elastic cross sections for electron impact on the OCS target molecule in the gas phase. In particular, we have employed the exact description of the static potential and a separable representation of the exchange potential, both represented via a single-center expansion, and we have further added correlation-polarization effects via a density functional formulation that we have discussed many times before [17]. The corresponding integro-differential equations

have been solved via quadratures of Volterra equations as discussed in section II and the angular distributions have been computed including the Born dipole corrections beyond the partialwave value of  $l_{max}=30$  [20]. The final results for the integral cross sections indeed confirm the presence, around 1 eV of collision energy, of a narrow and intense shape resonance of  $\Pi$ -symmetry associated to a well-known  $\pi^*$  resonance for the title system (e.g- see discussion in ref.s[7, 9]. It also suggests the presence of further two resonances of  $\pi^*$  and  $\sigma^*$  symmetry and larger widths, together with a clear Ramsauer-Townsend minimum in the cross sections around 0.7 eV [10]. Furthermore, the various available angular distributions for the elastic scattering have also been analyzed over a very broad range of collision energies, spanning nearly 100 eV, and compared with the existing experiments and with the earlier calculations [8, 9, 10]. The comparison of all the distribution data were presented in the previous Section and they show fair agreement between the measurements and with other computations [8, 9, 10]. The present calculations also show particularly good correspondence between computed and measured distributions for energies from 3.0 eV and up to 100 eV. Considering the complex, many-electron structure of the target and the broad range of collision dynamics which has been analyzed, our results do indicate the robustness of the adopted dynamical integrator and the reliability of the theoretical modelling which we have employed in this study.

## V. ACKNOWLEDGEMENTS

We thank the University of Rome, the Caspur Supercomputing Consortium and the COST Project "EIPAM" for financial and computational support during the carrying out of the present work.

- 
- [1] e.g. see: E.F. Van Dishoeck, in *The Molecular Astrophysics of Stars and Galaxies*, T.W. Harthwuist and D.A. Williams Ed.s, Oxford Scientific, N.Y. (1998).
  - [2] M.G. Lynch, D. Dill, J. Siegel and J.L. Dehmer, *J.Chem. Phys.*, **71**,4249 (1979).
  - [3] W. Sohn, K.-H. Kochem, M. Scheuerlein, K. Jung and H. Ehrhardt, *J. Phys. B*, **20**,3217 (1987).
  - [4] C. Zmytkowski, G. Karwasz and K. Maciag, *Chem. Phys. Lett.*, **107**, 481 (1984).
  - [5] H. Tanaka, private communication (1999).
  - [6] M.K. Kawada, O. Sueoka and M. Kimura, *J.Chem. Phys.*, **112**, 7057 (2000).

- [7] M.H.F. Bettega, M.A.P. Lima and L.G. Ferreira, *Aust. J. Phys.*, **53**, 399(2000).
- [8] S.E. Michelin, T. Kroin, I. Iga, M.G.P. Homem, M.S. Miglio and M.T. Lee, *J. Phys. B*, **33**, 3293(2000).
- [9] M.H.F. Bettega, M.A.P. Lima and L.G. Ferreira, *Phys. Rev. A*, **70**, 062711(2004).
- [10] M.H.F. Bettega, M.A.P. Lima and L.G. Ferreira, *Phys. Rev. A*, **72**, 014702(2005).
- [11] T.N. Rescigno and A. Orel, *Phys. Rev.A*, **24**, 1267(1981);*Phys. Rev.A*, **25**, 2402(1982) .
- [12] F.A. Gianturco and T. Stoecklin,*J. Phys.B*, **27**, 5903 (1994).
- [13] F.A. Gianturco, R. Curik and N. Sanna, *J. Phys. B*, **33**,2705 (2000).
- [14] L. Malegat, M. Le Dorneuf and V.K. Lan, *J. Phys. B*, **20**,4143 (1987).
- [15] A. Jain and D.W. Norcross, *Phys. Rev. A*, **32**,1341 (1985).
- [16] T.H. Dunning Jr. and P.J. Hay, in *Modern Theoretical Chemistry*, H.F. Schaefer III Ed., Vol. 3, Plenum Publ., New York (1967).
- [17] e.g. see: I.I. Fabrikant, *J. Phys. B*, **14**,335 (1981).
- [18] W. Vannroose, C.W. McCurdy and T.N. Rescigno, *Phys. Rev.A*, **68**, 052713(2003).
- [19] e.g. see: F.A. Gianturco, R.R. Lucchese, N.Sanna and A. Talamo, in *Electron Collisions with Molecules, Clusters and Surfaces*, H. Ehrhardt and L.A. Morgan Ed.s, Plenum Publ., New York (1994).
- [20] e.g. see: Y. Itikawa, *Theor. Chem. Acc.*, **105**, 123(2000).

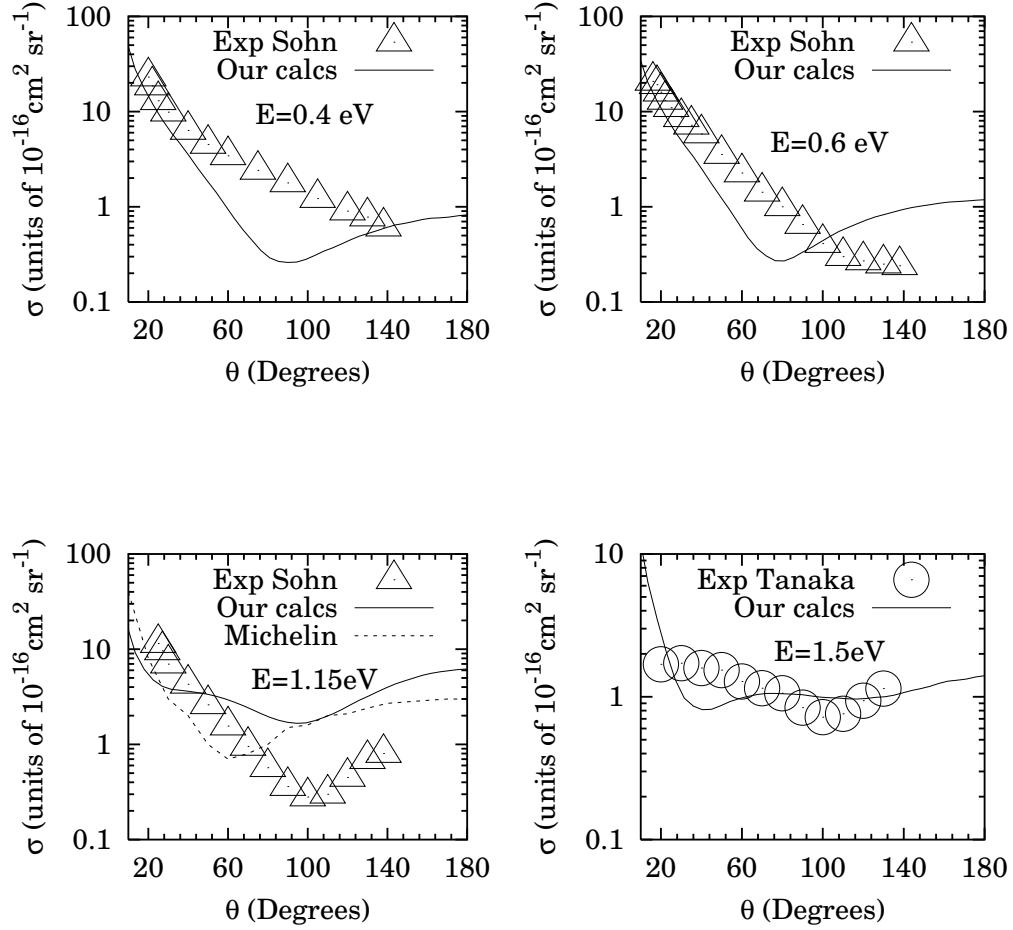


FIG. 3: Computed and measured angular distributions. Solid line: present calculations, open triangles: expt.s from ref.[3]. Open circles: expt.s from ref.[5], dashes: calculations from ref.[8]. Upper left panel: 0.4 eV. Upper right panel: 0.6 eV. Lower left panel: 1.15 eV. Lower right panel: 1.5 eV.

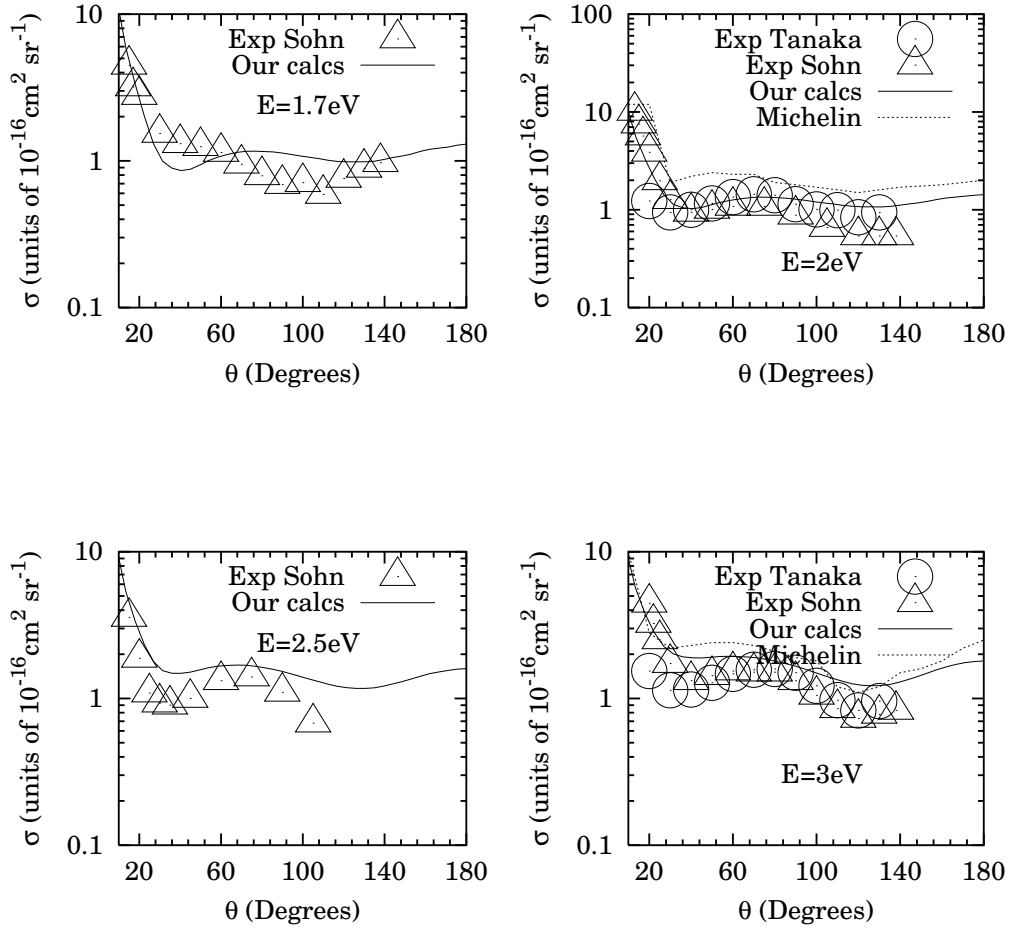


FIG. 4: Same as in figure 3 but for different collision energies. The dashed lines are calculations from ref.[8]. Upper left panel: 1.7 eV; upper right panel: 2.0 eV; lower left panel: 2.5 eV; lower right panel: 3.0 eV.

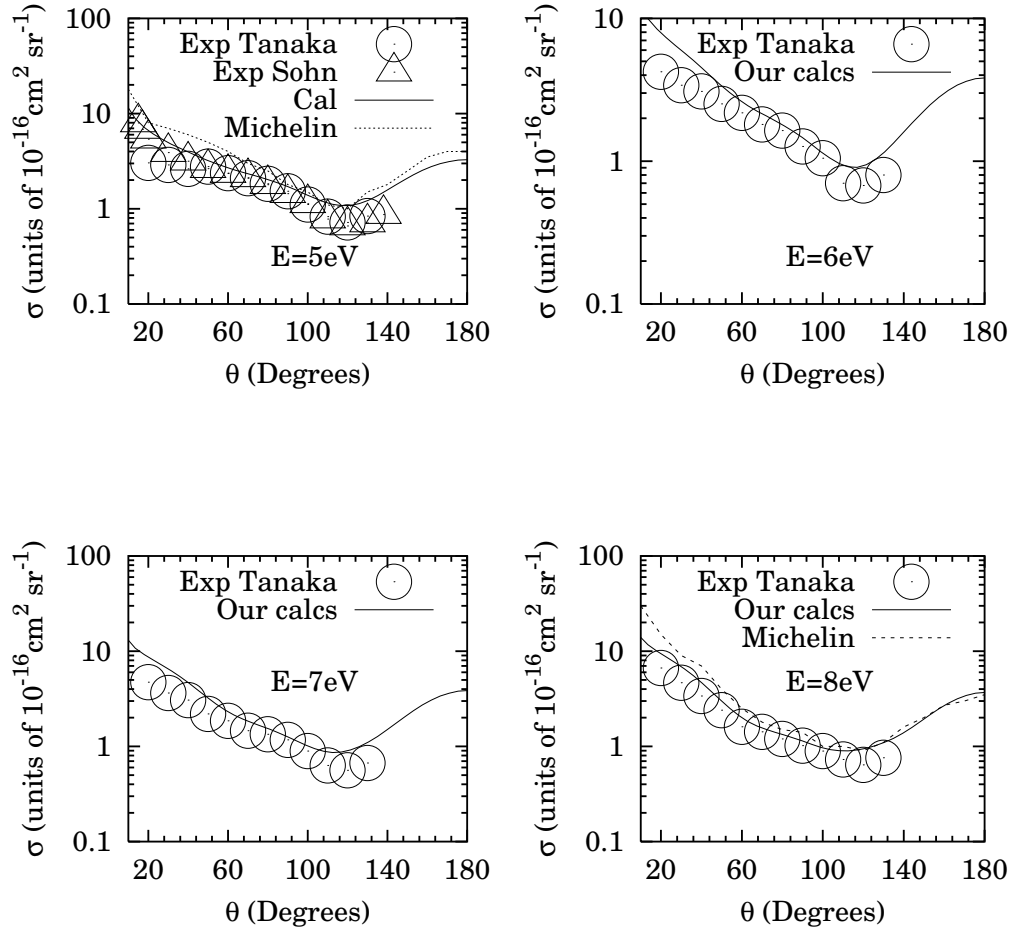


FIG. 5: Computed and measured angular distributions. Solid lines: present calculations. Dashes: calculations from ref.[8]. Open circles: expt.s from ref.[5]; triangles: expt.s from [3]. Upper left panle: 5.0 eV. Upper right panel: 6.0 eV. Lower left panel: 7.0 eV. Lower right panel: 8.0 eV.



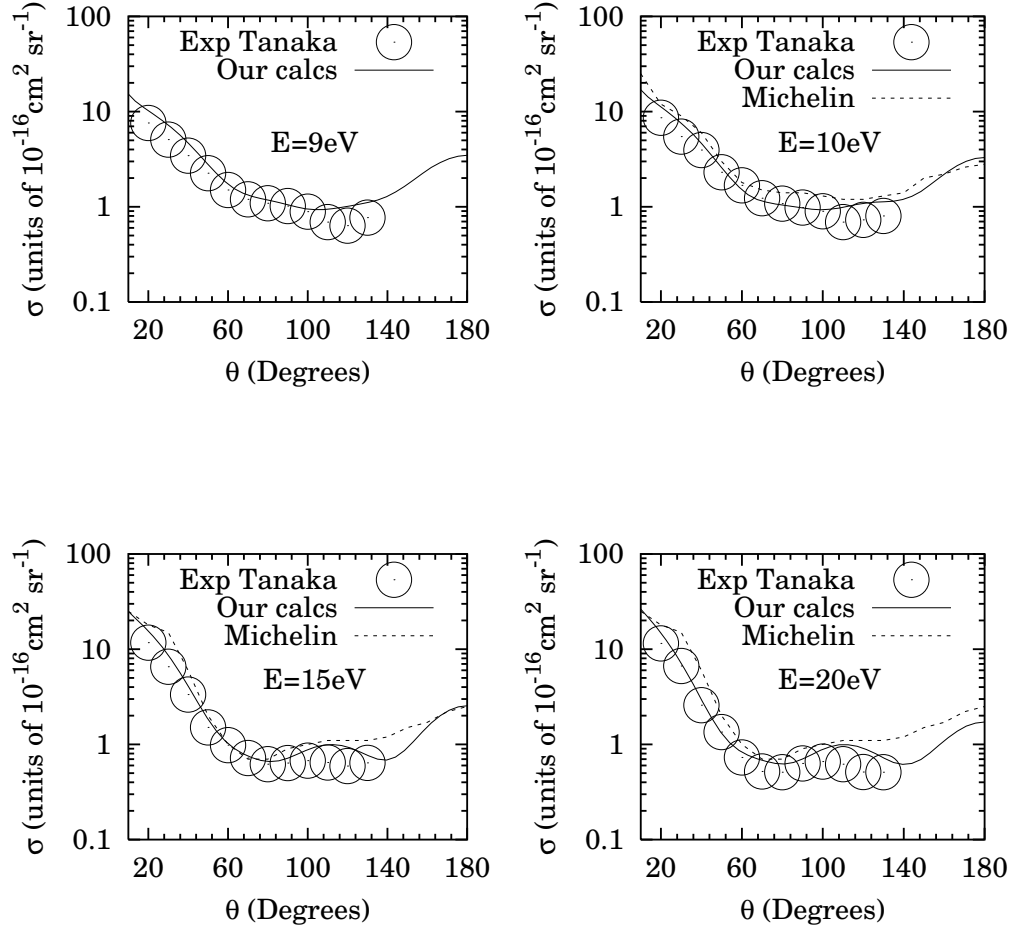


FIG. 6: Same as in figure 5 but for different collision energies. Upper left panel: 9.0 eV; upper right panel: 10.0 eV; lower left panel: 15 eV; lower right panel: 20.0 eV.

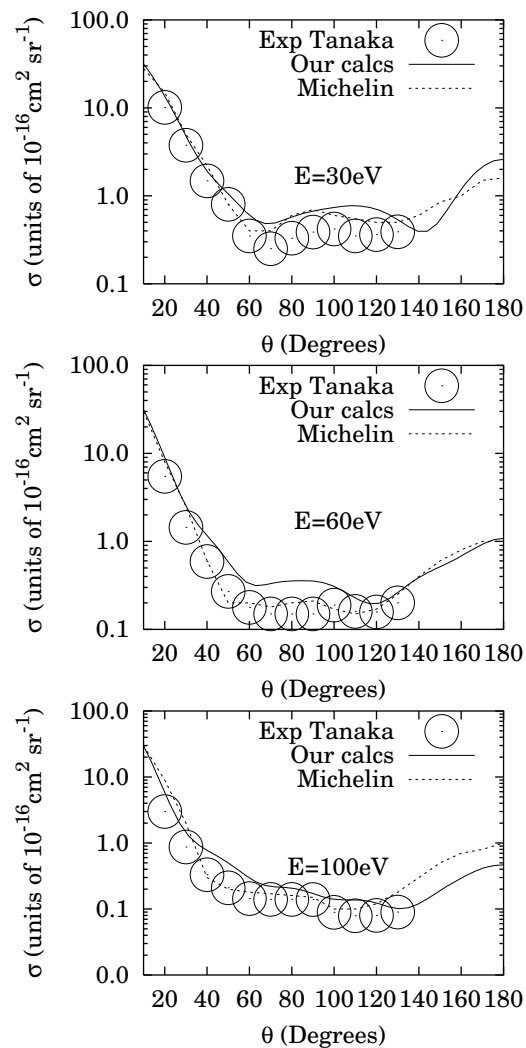


FIG. 7: Same as in figure 6 but for different collision energies, Upper left panel: 30.0 eV. Middle panel: 60.0 eV. Lower panel: 100.0 eV.